

RESEARCH ARTICLE

10.1029/2019JB018469

Key Points:

- The Turkana Depression accommodates divergence through localized extension
- African extension is accommodated by a combination of high and low strain rates
- Topographic gradients appear to influence the style of extension throughout the African rift system

Supporting Information:

- Supporting Information S1
- Supporting Information S2

Correspondence to:

E. Knappe,
ellen.knappe@umontana.edu

Citation:












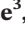
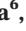


Knappe, E., Bendick, R., Ebinger, C., Birhanu, Y., Lewi, E., Floyd, M., et al. (2020). Accommodation of East African Rifting across the Turkana Depression. *Journal of Geophysical Research: Solid Earth*, 125, e2019JB018469. <https://doi.org/10.1029/2019JB018469>

Received 31 JUL 2019

Accepted 30 JAN 2020

Accepted article online 12 FEB 2020

Accommodation of East African Rifting Across the Turkana Depression

E. Knappe¹ , R. Bendick¹ , C. Ebinger² , Y. Birhanu¹ , E. Lewi³ , M. Floyd⁴ , R. King⁴ , G. Kianji⁵ , N. Mariita⁶ , T. Temtime⁷ , B. Waktola³ , B. Deresse³ , M. Musila⁶ , J. Kanoti⁵ , and M. Perry¹ 

¹Department of Geosciences, University of Montana, Missoula, MT, USA, ²Earth and Environmental Sciences, Tulane University of Louisiana, New Orleans, LA, USA, ³Institute of Geophysics, Space Science and Astronomy, Addis Ababa University, Addis Ababa, Ethiopia, ⁴Department of Earth, Atmospheric and Planetary Sciences, Massachusetts Institute of Technology, Cambridge, MA, USA, ⁵Department of Geology, University of Nairobi, Nairobi, Kenya, ⁶Geothermal Energy Training and Research Institute, Dedan Kimathi University of Technology, Nyeri, Kenya, ⁷School of Earth Sciences, University of Bristol, Bristol, UK

Abstract Geodetic observations in the Turkana Depression of southern Ethiopia and northern Kenya constrain the kinematic relay of extension from a single rift in Ethiopia to parallel rifts in Kenya and Uganda. Global Position System stations in the region record approximately 4.7 mm/year of total eastward extension, consistent with the ITRF14 Euler pole for Nubia-Somalia angular velocity. Extension is partitioned into high strain rates on localized structures and lower strain rates in areas of elevated topography, as across the Ethiopian Plateau. Where high topography is absent, extension is relayed between the Main Ethiopian Rift and the Eastern Rift across the Turkana Depression exclusively through localized extension on and immediately east of Lake Turkana (up to 0.2 microstrain/year across Lake Turkana). The observed scaling and location of active extension in the Turkana Depression are inconsistent with mechanical models predicting distributed stretching due to either inherited lithospheric weakness or reactivated structures oblique to the present-day extension direction.

Plain Language Summary The continent of Africa is breaking up into multiple pieces. This divergence is accommodated through extension along the East African Rift System. The Turkana Depression, which lies on the border of Ethiopia and Kenya, is of interest due to its previous rifting episodes, low elevation compared to the surrounding rift system, and location linking more prominent rift valleys to the north and south. Global Position System observations of surface velocities show that extension in the Turkana Depression is confined to a narrow region, not distributed across a broad area. These results suggest the East African Rift System is accommodating the breakup of the African continent through a combination of distributed deformation in areas with high topography and localized extension across low elevation rift basins.

1. Introduction

Active deformation in the seismically and volcanically active East African Rift System (EARS) exemplifies the processes of cratonic lithospheric breakup. Composed of a series of diachronous volcanic provinces and fault-bounded basins, the continent-scale EARS accommodates the relative motion of the Somalia plate away from the Nubia plate, dividing the African continent into at least two blocks. In this context, along-strike comparisons of strain distribution between areas with and without magmatism, within or far from the broad plateau uplifts, and in lithosphere with varying preexisting architecture enable bounding constraints on the relationship between gravitational potential energy (GPE), rheology, and strain localization.

From north to south, the EARS starts at the triple junction in the southernmost Afar Depression and transitions into the younger and structurally distinct Main Ethiopian Rift (MER). The MER is separated from the parallel rift structures of the Western Rift and the Eastern Rift (Kenyan/Gregory Rift and the Northern Tanzania Divergence) by the Turkana Depression. The Depression lies in a topographic low where the earliest East African magmatism and faulting is thought to have initiated based on comparison of volcanic and sedimentary rock ages throughout the region (Figure 1) (e.g., Brown & McDougall, 2011; Morley, Wescott, et al., 1999; Wolfenden et al., 2004).

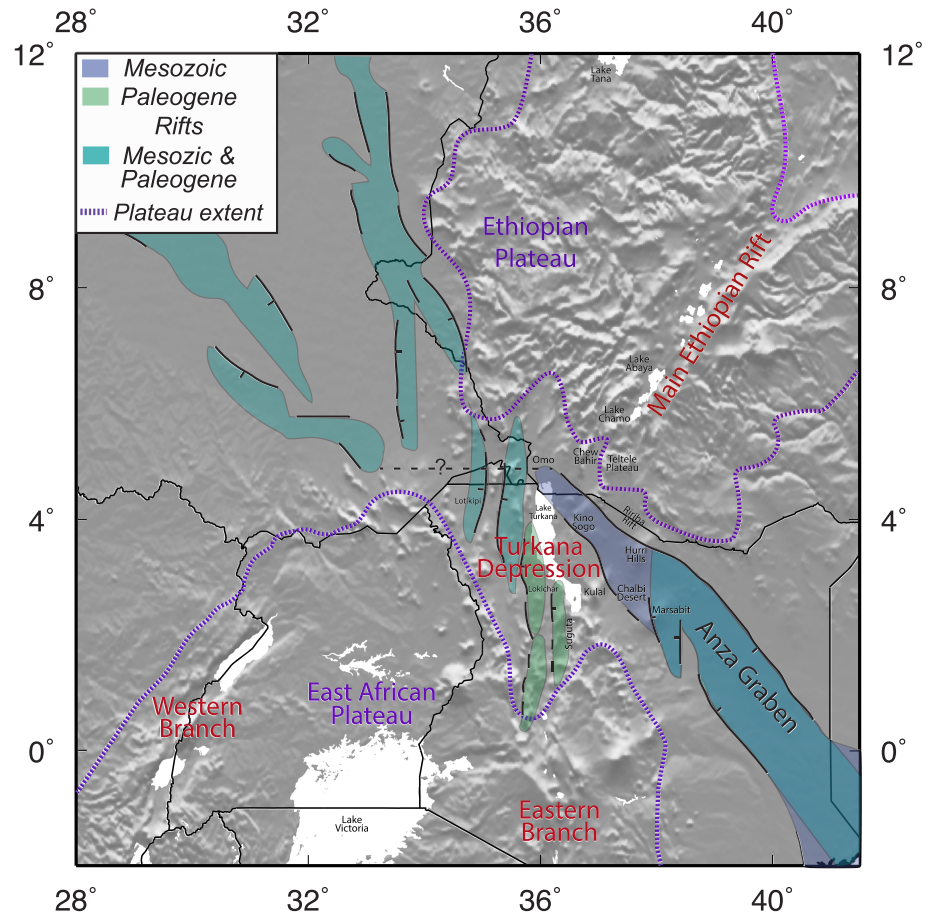


Figure 1. Past rifting and plateau extent in and around the Turkana Depression. Lateral extent of rifts from the Paleogene era (green) and the Mesozoic era (blue) and rifts that were active during both periods (blue-green) that traverse the Turkana Depression. Boundaries of Paleogene, and Mesozoic rifts from gravity analyses (Ebinger & Ibrahim, 1994) and exploration data (Bosworth, 1992; Bosworth & Morley, 1994). Timing of basin initiation in Lotikipi constrained to L. Cretaceous-Paleogene (Morley, Day, et al., 1999; Morley, Wescott, et al., 1999; Wescott et al., 1999; Tiercelin et al., 2012). The basins to the west of the southern portion of Lake Turkana (including the Lokichar Basin) were also active during L. Paleogene into the mid-Miocene (Morley, Day, et al., 1999; Morley, Wescott, et al., 1999; Wescott et al., 1999; Tiercelin et al., 2012). Hashed purple lines outline the Ethiopian and East African plateaux. Present-day EARS segments are labeled in red and locations referred to in the text are labeled.

The high topography of the EARS is consistent with the presence of a large, low-density upwelling rising from the core-mantle boundary to beneath the lithosphere, indicated by seismic, geochemical, and thermal data (e.g., Bastow et al., 2008; Furman et al., 2006; George et al., 1998; Sippel et al., 2017). The large-scale mantle upwelling and presence of lithospheric thickness variations at the onset of rifting explain flood magmatism and continent-scale rifting in the absence of far-field slab-pull forces south of the Red Sea (e.g., Ebinger & Sleep, 1998). GPE created by low density material in the mantle, as well as flexural uplift of initially strong, cold lithosphere along the flanks of rift basins is a critical component of the force balance for the entire EARS (Coblentz & Sandiford, 1994; Kendall & Lithgow-Bertelloni, 2016; Stamps et al., 2014).

Present-day total extension rates in the MER are estimated between 5 and 7 mm/year (Birhanu et al., 2016; DeMets et al., 2010; Saria et al., 2014; Stamps et al., 2008), decreasing monotonically southward, consistent with a Nubia-Somalia Euler pole south of the African continent (e.g., DeMets & Merkouriev, 2016). This extension is not confined within the fault-bounded rift valley in Ethiopia but is instead a combination of more localized (high strain rate) stretching on either magmatic segments or on rift bounding faults, and more distributed (low strain rate) stretching across the western portion of the Ethiopian Plateau (Birhanu et al., 2016). The distributed deformation across the plateau is coincident in space with both high

elevation and low effective lithospheric viscosity (Chambers et al., 2019; Jay et al., 2015). Southward, the Western and Eastern Rifts define the sides of the ~1,500-m-high East African Plateau. Geodetic extension rates across each rift are estimated to be between 1 and 5 mm/year, with kinematic relay between structures resulting in extensional velocities increasing southward in the Western Rift and decreasing southward in the Eastern Rift (e.g., Saria et al., 2014; King et al., 2019). While the Western Rift is relatively amagmatic, the MER and Eastern Rift are characterized by magmatism since rift initiation, which occurs within and outside the rift valleys, and has been shown to accommodate extension in both rifts (e.g., Vetel & Le Gall, 2006; Corti, 2009; Rooney, 2017).

The Turkana Depression is a critical location to constrain the kinematic budget for relaying EARS extension from the MER to the parallel Western and Eastern Rifts. It additionally provides the opportunity to test the influence of gravitational potential and material properties in controlling the style and scaling of strain accommodation. The Depression spans the complex structural domain between well-defined rift structures. It has little topographic relief (mean elevation of 500 m) and contains inherited lithospheric structures from past rifting episodes, providing mechanical constraints. Because the gradient in body forces across the depression is very low, contributing little to the lithospheric dynamic state, the region also defines a low-GPE end-member for the dynamics of continental rifting. The superposition of at least two phases of rifting in the Mesozoic and Oligo-Miocene to Recent time produced a region of enhanced crustal thinning with crustal thickness of only 20 km beneath Lake Turkana, compared to the 27–35 km beneath the Eastern and MERs (Ebinger et al., 2017; Hendrie et al., 1994; Mechie et al., 1994; Sippel et al., 2017). The NW-SE trending Mesozoic rift structures of the Anza and SE Sudan rifts are oblique to the present-day extension direction, and their reactivation has been invoked as an alternative cause of a lack of uplifted footwalls in parts of the Turkana Depression (Brune et al., 2017; Boone et al., 2018).

In this study, we measure present-day geodetic surface velocities, calculate the partitioning of extension among the MER and northern portions of the Western and Eastern rifts, and explore the importance of both GPE and inherited lithospheric structures to rift architecture, morphology, and strain rate.

1.1. Magmatism and Extension in the Turkana Depression

Evidence of extension in the Turkana Depression dates back to the Cretaceous, when the NW-SE trending Anza Rift extended through northern Kenya, although its connection across eastern Sudan to connect with the Mesozoic Central Africa Rift remains ambiguous owing to data gaps in South Sudan (Figure 1) (Bosworth & Morley, 1994; Ebinger & Ibrahim, 1994; Hendrie et al., 1994; Morley, Day, et al., 1999). During this period, volcanism was limited to E-W trending dykes along strike-slip faults connecting southern Ethiopia into South Sudan (Ebinger et al., 1993) and eastward to the Anza Graben (Morley, Day, et al., 1999; Morley, Wescott, et al., 1999). In the Paleogene, reactivation of the Anza Rift and extension west of present-day Lake Turkana occurred (Boone et al., 2019; Bosworth, 1992; Bosworth & Morley, 1994; Ebinger & Ibrahim, 1994; Morley et al., 1992; Morley, Wescott, et al., 1999; Wescott et al., 1999). Magmatism in southern Ethiopia then began in the late Eocene, and by 45–35 Ma was widespread in southern Ethiopia and in the Lotikipi-Lapurr and proto-Kino Sogo regions of Kenya (e.g., Davidson & Rex, 1980; Ebinger et al., 1993; Morley, Wescott, et al., 1999; Vetel & Le Gall, 2006). During the Eocene and into the Oligocene (39–35 Ma), bimodal volcanism in northern Kenya and basaltic activity in southern Ethiopia continued with initiation of the oldest half grabens on the west side of the present-day lake (Ebinger et al., 1993; Vetel & Le Gall, 2006). Widespread rifting in the Turkana Depression began at 25 Ma with a second, more voluminous, phase of volcanism (Furman et al., 2006; Morley et al., 1992), with basin subsidence and rapid infill occurring by 20–18 Ma (Morley, Wescott, et al., 1999). In the lower Miocene, volcanism and extension migrated eastward (Vetel & Le Gall, 2006).

At 20 Ma, chemical and thermal anomalies in lavas indicate impingement of a plume beneath Turkana and initial uplift of the Ethiopian Plateau (Figure 1) (Furman et al., 2006; Pik et al., 2008). In southern Ethiopia, basaltic activity and extension migrated northward with faulting and basin development in the southern MER between 18 and 14 Ma (Balestrieri et al., 2016; Ebinger et al., 1993; Ebinger et al., 2000). Extension and magmatism initially continued in place in the Turkana Depression, migrating southward only in the upper Miocene (Morley et al., 1992; Morley, Wescott, et al., 1999; Vetel & Le Gall, 2006). The Turkana Depression also has the largest spatial expanse of Miocene-Recent lavas (>120,000 km²; Guth, 2016), with sedimentary basins containing 2 km or more of eruptive material (Guth, 2016; Morley et al., 1992) and

intrusive volumes three or more times larger than the eruptive volumes based on studies in other EARS rift sectors (e.g., Ebinger et al., 2017). Lateral compositional variations are, therefore, expected across the Turkana Depression. Localized faulting and basaltic activity in the Suguta rift segment began in the Early Pliocene (Bosworth & Maurin, 1993).

Present-day volcanism is more restricted to basaltic shield complexes within the Turkana Depression, with geochemical evidence of both lithospheric and sublithospheric contributions (Furman et al., 2004; Kaeser et al., 2006; Rooney, 2017). Seismic reflection and gravity surveys reveal east-dipping half-grabens beneath the Turkana Depression, with the largest offset faults occurring beneath and adjacent to the southwest portion of Lake Turkana (Dunkelman et al., 1989; Morley et al., 1992; Morley, Wescott, et al., 1999). These studies estimate 25–40 km of total extension with β stretching factor of 1.55–1.65 (Hendrie et al., 1994; Morley et al., 1992). Based on present-day fault structures mapped in the region, modern extension is believed to be confined to the southern Lake Turkana, Kino Sogo, Ririba, and Suguta rift segments (e.g., Dunkelman et al., 1989; Bosworth & Maurin, 1993; Vetel & Le Gall, 2006).

Plate kinematic models of the EARS allow total relative extension between 4.3 and 3.1 mm/year (Stamps et al., 2008; Saria et al., 2014) in the Turkana segment, but such estimates are highly sensitive to block geometry (e.g., Stamps et al., 2008; Stamps et al., 2014). The Turkana Depression has high heat flow compared to the surrounding regions, consistent with widespread magmatism (Morley, Wescott, et al., 1999; Sippel et al., 2017). Effective elastic thickness in the depression have been estimated at 5–20 km (Hendrie et al., 1994; Ebinger, 1989). A more detailed timeline of the magmatism and extension and the locations of activity in the Turkana Depression are provided in the supporting information Figures S1 and S2.

2. Methods

To constrain the present-day surface kinematics in the Turkana Depression, we installed eight campaign and two continuous Global Position System (GPS) stations, spanning from south of Lake Chamo, Ethiopia, to Samburu County, Kenya, across the region of documented active deformation (pink stations in Figure 2). The network spans the area surrounding Lake Turkana as well as the Omo-Chew Bahir-Weyto regions of southern Ethiopia, sometimes referred to as the Broadly Rifted Zone. Campaign sites were measured in 2014, 2017, and 2019, and continuous sites were installed on the eastern and western shores of Lake Turkana in 2017. Sites are arranged in three roughly rift-normal lines, with spacing between station pairs of 200 to 300 km. Security concerns limit the array aperture to the west near South Sudan. Campaign sites consist of stainless steel dimpled monument pins installed in bedrock and measured using bipod mounts for 2- to 7-day epochs. Continuous sites consist of shallow driven-braced monuments in sediment.

Observations from the study network are combined with data collected from 2012 to 2019 at 12 continuous and eight campaign GPS stations in Ethiopia and Kenya, plus International GNSS Service (IGS) continuous stations in Africa, Europe, and Asia for registration to a standard global reference frame. These data are processed using GAMIT/GLOBK analysis software (Herring et al., 2010) following the approach described by Reilinger et al. (2006). GAMIT loosely estimates satellite, atmospheric, orbital, phase parameters, and station coordinates from the raw observations. These estimates and their covariances are then combined with daily global solutions provided by MIT to generate position time series. The time series are edited for outliers and offsets before determining appropriate weighting for individual stations. For campaign stations, which have too few observations to develop a site-specific noise model, the median noise model from the continuous stations ($e, n, u = 1.33e-7, 2.08e-7, 31.28e-7, m^2/year$) is applied. One millimeter of additional white noise is added to the daily position estimates, which are then aggregated into approximately 14-day averages. GLOBK fits these 14-day averages using a Kalman filter to estimate site velocities in the International Terrestrial Reference Frame (ITRF2014) (Altamini et al., 2016). The velocity solution is then combined with the GeoPRISMS-sponsored community geodetic velocity solution, which includes additional stations in the region (King et al., 2019, doi:10.1594/IEDA/324785). The combination of the two solutions is done by estimating a frame transformation using 14 common stations (RMS for all 28 components is 0.26 mm/year; additional information included in Table S2). The merged velocity field is finally transformed into a Nubia-fixed frame using the ITRF2014-Nubia rotation vector (Altamini et al., 2017). The final velocity solution excludes sites with known monumentation problems and stations with poorly determined positions (1-sigma uncertainties larger than 1.5 mm/year).

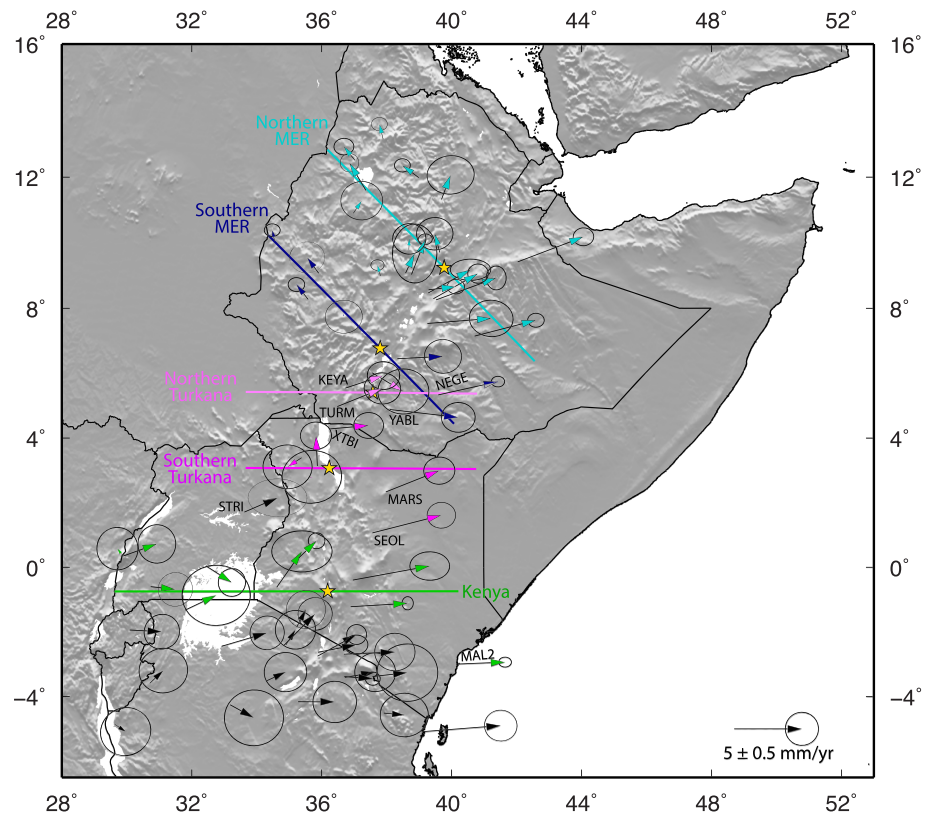


Figure 2. Velocity solution in a Nubia-fixed reference frame with 95% confidence ellipses. Stations are separated into five transect (represented by the five colored lines with their names in the same color). Stations are color coded by their associated transect. Transects and color scheme used in Figures 3 and 4. Stars indicate the location of maximum strain rate (defined by the inflection point (x_{d^2v/dx^2})) in the sigmoid fit in equation (1)). The transects are rift normal and 900 km long, with the exception of the Kenya Profile, which is 1,200 km. Stations mentioned in the text are labeled.

Next, site velocities are separated into five rift-normal transects and the east component of velocity is plotted as a function of profile distance, since the principal extension direction has been estimated between 85° and 105° (e.g., Altamimi et al., 2012; Kogan et al., 2012; Saria et al., 2013). A sigmoid function

$$v_x = v_{min} + \frac{v_{max}}{1 + \exp\left(\frac{x_{d^2v/dx^2} - x}{\rho}\right)} \quad (1)$$

is fit to the profiles, following Kogan et al. (2012), using the uncertainties as weights, where v_x is the velocity, v_{min} is the minimum velocity, v_{max} is the maximum extension velocity, x_{d^2v/dx^2} is the x -coordinate of the inflection point of the sigmoid, and ρ is the sigmoid rate coefficient. The 1-D spatial derivative of each sigmoid, $\frac{\partial v}{\partial x}$ approximates the strain rate across the profile. Since the Southern MER and Northern Turkana profiles cross near station NEGE, both profiles contain station NEGE. In the Kenya profile, the profile observations are augmented with the addition of IGS station MAL2 to pin the profile end to the full Somalia relative velocity.

3. Results

The regional velocity solution, relative to stable Nubia, shows the ongoing divergence between Nubia and Somalia (Figure 2 and Table S1). The magnitude, orientation, and spatial scaling of velocity gradients provide constraints on both how and where extension is relayed between well-defined structures north (MER) and south (Western and Eastern rifts) of the Turkana Depression and the material properties and body forces in the Depression that influence the distribution of strain in the crust.

3.1. Kinematics

In the first case, the five velocity transects and the least-squares sigmoid approximation to the 1-D velocity profiles reveal the kinematic budget of the Turkana Depression and its connection to the rest of the EARS (Figures 3 and 4). In particular, the magnitude of the total extensional velocity and the location of extension in space show which structures accommodate Nubia-Somalia relative motion in Turkana. In the continuous sigmoid fits, these values are represented by $v_{max} - v_{min}$ and x_{d^2v/dx^2} , respectively (Table 1).

In the northern MER, the maximum extension rate (v_{max}) is 5.6 ± 0.3 mm/year (Figures 3a and 4a—light blue in all profiles). This is consistent with the instantaneous local velocity calculated from the relative plate motion between Nubia and Somalia, defined by ITRF2014 Euler poles, of 5.7 mm/year. Maximum extension in the southern MER is slightly less than in the northern MER sector, with $v_{max} = 5.0 \pm 0.3$ mm/year, also consistent with the slightly smaller extension rates derived from ITRF2014 Euler pole calculations of 5.3 mm/year (Figures 3b and 4a—dark blue in all profiles). In both cases, extension is centered on the well-defined fault bounded rift valley, but diffuse deformation also occurs across the western part of the Ethiopian Highlands as described in Birhanu et al. (2016).

The Northern Turkana profile has a minimum velocity (v_{min}) of 2.6 mm/year due to limited station distribution along the eastern margin of the Depression near South Sudan (Figures 3c and 4a—light pink in all profiles). The lack of stations on stable Nubia means this profile does not capture the full divergence between Nubia and Somalia. This profile directly captures only the 1.9 mm/year of extension across the Chew Bahir rift and its uplifted flank, the Teltele Plateau, between stations TURM/KEYA and YABL.

The Southern Turkana profile does include stations on stable Nubia, demonstrating that this profile captures the full divergence of Nubia and Somalia (Figures 3d and 4a—dark pink in all profiles) as stations to the west of Lake Turkana have negligible velocities in a Nubia-fixed frame. Maximum extension velocity across the profile (v_{max}) is 4.7 ± 0.4 mm/year, consistent with ITRF2014 calculations (5.1 mm/year). We do not include the station STRI in this profile since it is located in central Uganda on the East African Plateau, south of the southern tip of Lake Turkana, and records an eastward velocity of 2.4 ± 0.9 mm/year. The position of STRI and its nonzero eastward velocity likely captures extension in the Western rift on structures that bound Lake Albert or across a portion of the East African Plateau. Since the stations on the west side of Lake Turkana record a Nubia fixed velocity, we pin the end of the profile to the Nubia fixed velocity and include the frame uncertainty (0.0 ± 0.28 mm/year).

The central Kenya profile also does not capture the complete divergence of Nubia and Somalia. Instead, the Kenya profile, which starts east of the Western rift (due to lack of stations in Uganda), has a minimum velocity (v_{min}) of 1.6 ± 0.2 mm/year, further demonstrating extension across the Western rift or East African Plateau (Figures 3e and 4a—light green in all profiles). Thus, the Kenya profile is primarily measuring extension across the Eastern rift, where velocities increase by 2.6 ± 0.3 mm/year.

3.2. Dynamics

The spatial derivatives of the continuous 1-D sigmoid curves approximate the strain rate across each profile (Figure 4b). Through comparisons to other segments of the EARS, these strain rate models provide a bounding constraint on the influence of GPE to the characteristic scaling of EARS rifting. In the continuous sigmoid fits, the distance over which finite extension is distributed is represented by the rate coefficient, ρ . The distance over which the derivative (strain rate) is greater than 2.5% of the maximum strain rate can therefore be used to determine a consistent characteristic length scale for comparisons among rift segments.

In the northern MER, extension is accommodated over a large distance, with a rate coefficient of 52.5 (Figure 4) corresponding to finite strain rates over a minimum of 500 km. Due to lack of stations near the Ethiopia/Somalia border this length scale is itself a lower bound. Finite strain over hundreds of kilometers requires nonphysical locking depths of greater than 100 km for a single dislocation (see Figure S4) or several closely spaced dislocations with very small displacements which have not been documented in the MER. The Southern MER similarly displays distributed extension, with a rate coefficient of 53.9, and low strain rates across the profile also with a scale of at least 500 km (Figure 4). The highest strain rates in the northern and southern MER occur near the western rift-bounding fault (stars and yellow bars in Figures 2 and 3, respectively).

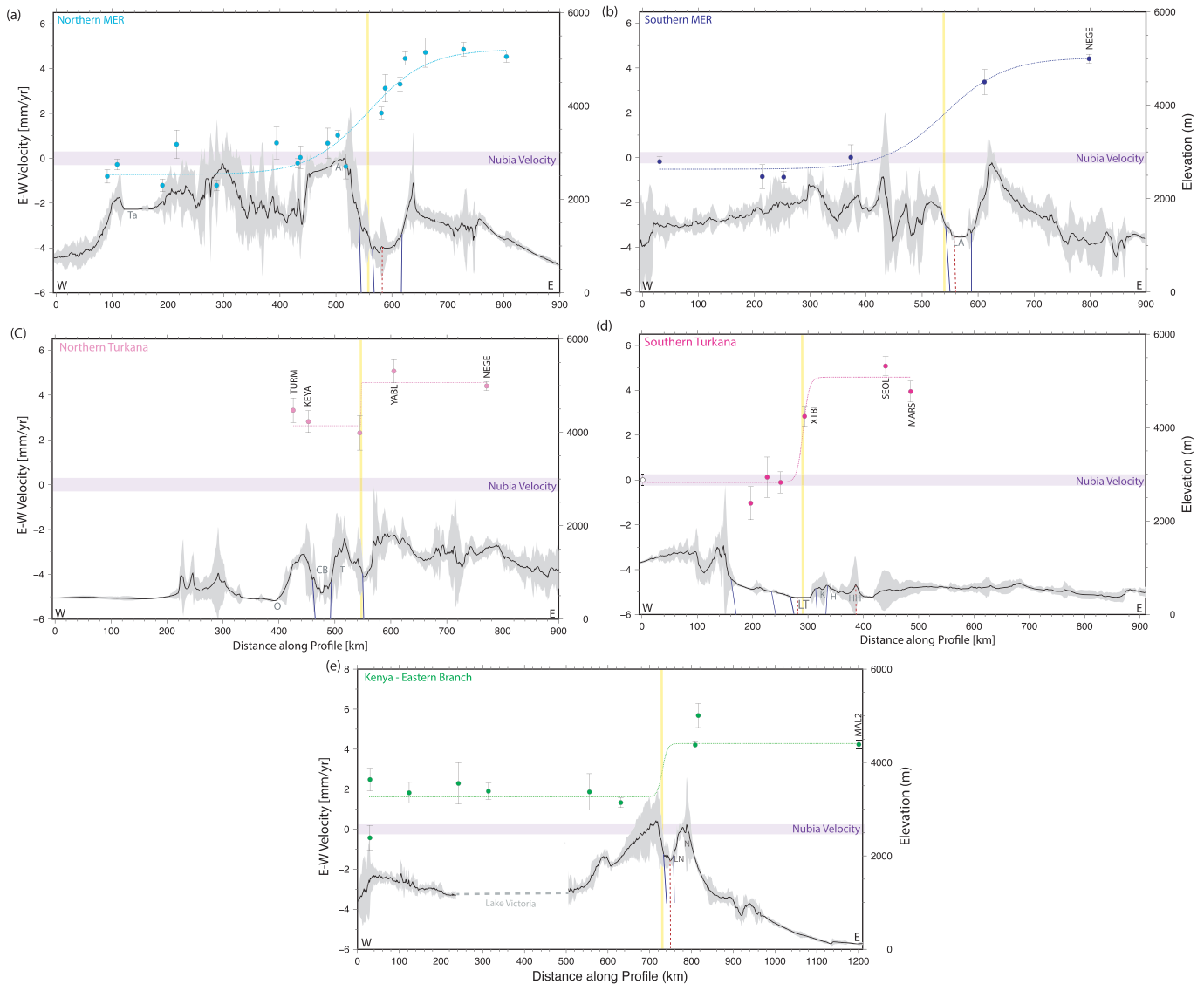


Figure 3. Velocity profiles. The east velocity magnitude (present-day extension direction) and 1 sigma uncertainty with topography swaths taken from 50 km on either side of the transect. Sigmoid fit (equation (1)) for each segment represented with dashed line. Profiles are oriented west to east with a) the Northern MER profile, b) the Southern MER, c) Northern Turkana, d) Southern Turkana, e) Kenya - Eastern Branch; location of transects are indicated on Figure 2. The expected Nubia velocity, and its uncertainty, defined by ITRF14 is shown with a light purple bar. Vertical yellow bar indicate the location of maximum strain rate (defined by the inflection point ($x_{d^2/y_{d^2}}$)) in the sigmoid fit—additionally labeled with a star in Figure 2). Landscape features in the profiles are labeled, including Ta = Lake Tana; A = Addis Ababa; LA = Lake Abaya; O = Omo River; CB = Chew Bahir; T = Teltele Plateau; LT = Lake Turkana; K = Kino Sogo Fault Belt; H = North Horr; HH = Hurri Hills; LN = Lake Navisha; N = Nairobi. Major faults indicated with blue lines and volcanic centers with dashed red lines (Ebinger et al., 2000; Morley et al., 1999; Vetel et al., 2005; Brune, 2016; Corti et al., 2018). Note the Kenya Profiles has slightly longer axes than the other four profiles to better view the data. Stations mentioned in text are labeled.

Unlike the MER profiles, both Turkana profiles show highly localized extension. The Turkana velocity gradients and strain rates are consistent with single elastic dislocations and shallow locking depths (Figure S4). The Northern Turkana profile shows extension occurring over a short distance, with a rate coefficient of only 0.02, causing the sigmoid function to approach a step function (Figure 4). The strain rate is correspondingly high, with a characteristic length scale of approximately 5 km (two orders of magnitude less than in the MER). This value neglects the ~ 2.6 mm/year of extension accommodated west of the end of the profile, so constrains the length scale and strain rate of only a portion of the total extension. The Southern Turkana profile also has a much higher strain rate than across the MER, with a rate coefficient of 5.5 indicating a length scale of extension of approximately 55 km, even while capturing the full Nubia-Somalia velocity (Figures 3

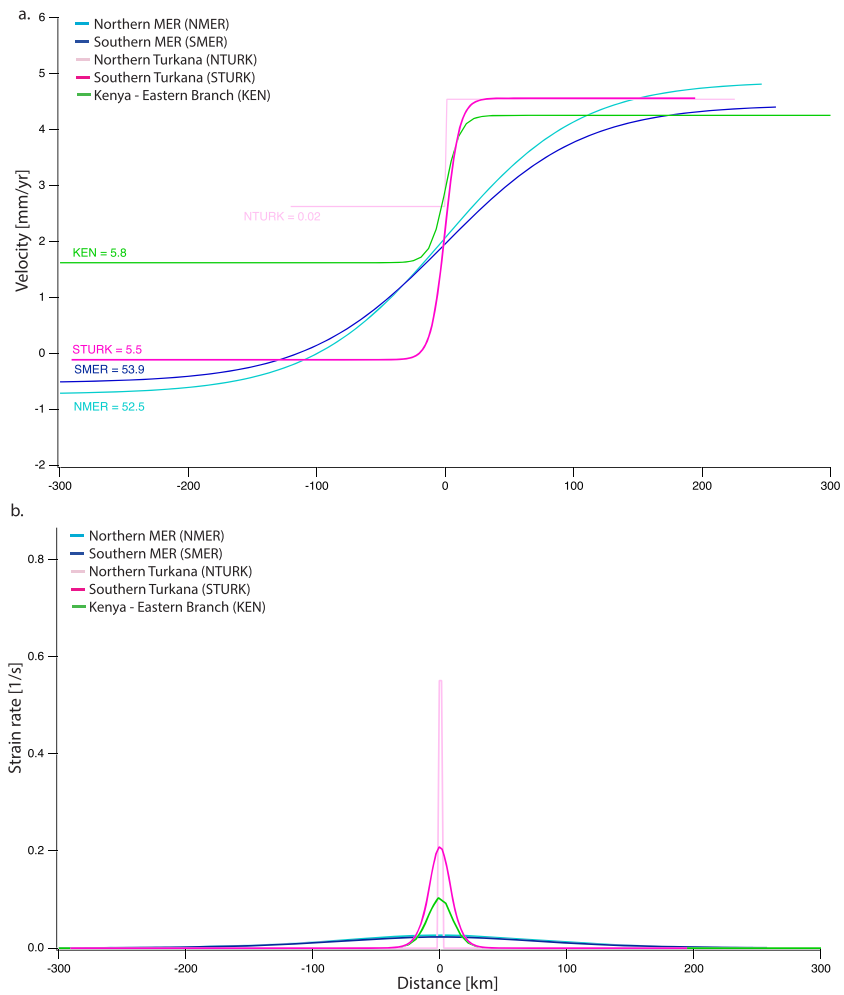


Figure 4. Sigmoid function fits and their derivatives (equation (1)). (a) Stacked sigmoid fits for all five profiles and their rate coefficients (ρ in equation (1)). Color-coding is the same as in Figure 3. (b) Stacked derivative of the sigmoid fit for each profile. All profiles (fit and derivative) are centered at their inflection point (x_{d^2-v/dx^2}).

and 4). The highest strain rates occur across Lake Turkana, which hosts two active volcanoes (Central and South Islands) (Figures 3 and 4). Excluding station XTBI from the profile because it is relatively far from the profile axis does not change the results; the characteristic length scale of extension remains 50 km with the highest strain rates across the lake (Figure S3).

In the Kenya profile, some of the total Nubia-Somalia extension is located west of the measured profiles, across the Western rift; these profiles constrain scaling only across the Eastern rift. The Kenya profile has

Table 1
The Coefficient Fits for the Sigmoid Function for All 5 Transects (Equation (1))

	v_{min}	v_{max}	x_{d^2-v/dx^2}	ρ
Northern MER	-0.7 ± 0.1	5.6 ± 0.3	558.3 ± 8.4	52.5 ± 6.6
Southern MER	-0.5 ± 0.2	5.0 ± 0.3	540.9 ± 53.5	53.9 ± 38.4
Northern Turkana	2.6 ± 0.3	1.9 ± 0.4	545.8^a	0.02^a
Southern Turkana	-0.1 ± 0.3	4.7 ± 0.4	291.0 ± 67.6	5.5^a
Kenya	1.6 ± 0.2	2.6 ± 0.3	730.7^a	5.8^a

^aInsufficient data points to accurately calculate formal uncertainty.

a rate coefficient of 5.8 and the characteristic length scale of finite rifting from the derivative is approximately 60 km, similar to the Turkana profiles and much smaller than in the MER (Figure 4). The highest strain rate in the profile occurs on the western edge of the rift structure (stars and yellow bars in Figures 2 and 3).

4. Discussion

4.1. Kinematics

The MER accommodates extension through both higher strain rate stretching within the fault-bounded rift and lower strain rate extension across the Ethiopian Highlands, consistent with previous geodetic studies of Ethiopia (Birhanu et al., 2016) (Figures 3a, 3b, and 4a). Total extension rates are consistent with plate tectonic models, with total relative Nubia-Somalia velocity of 5.6 mm/year in the northern MER, decreasing to 4.9 mm/year in the southern MER, also consistent with previous geodetic studies (Stamps et al., 2008; DeMets et al., 2010; Saria et al., 2014; Birhanu et al., 2016). As expected for a Nubia-Somalia Euler pole located south of the EARS, the total stretching velocity continues to decrease southward into the Turkana Depression and into the subparallel Western and Eastern rifts.

In the northern Turkana Depression, the maximum eastward velocity is 4.4 mm/year, again consistent with existing kinematic models (Stamps et al., 2008; Saria et al., 2014). Approximately 2.6 mm/year of extension must be accommodated west of the westernmost observations, possibly across the Omo Basin, or elsewhere in the southernmost Ethiopian Highlands (Figures 3c and 4a). An additional 1.9 mm/year of extension is accommodated across the Chew Bahir and Teltele Plateau, south of and along-strike with the MER. The current observations suggest the northernmost Turkana acts like an extension of the MER, with a combination of highly localized stretching on rift faults and eruptive centers, with additional extension perhaps distributed through the southernmost Ethiopian Highlands.

In the southern Turkana Depression, the three stations just to the west of Lake Turkana record Nubia fixed velocity ($v = 0$, Figures 3d and 4a), precluding any ongoing extension west of the lake-bounding faults. The negligible velocities at these stations require that the Paleogene basins west of lake are no longer actively accommodating extension, consistent with the eastward migration of magmatism and faulting inferred from earlier studies (Morley et al., 1992; Ebinger et al., 2000; Vetel & Le Gall, 2006). The kinematic budget also precludes an active enigmatic northward continuation of the Western rift into Turkana Depression, indicating the structures surrounding Lake Albert are likely the northernmost extent of the Western rift. Velocities relative to Nubia are nonzero immediately east of Lake Turkana, with station XTBI measuring an eastward velocity of 2.8 ± 0.5 mm/year, consistent with Nubia-Somalia divergence accommodated across and east of the lake (Ebinger et al., 2000; Vetel et al., 2005). Previous mapping studies suggest modern extension occurring across the Ririba Rift, which lies directly east of station XTBI (Bonini et al., 2005; Vetel et al., 2005; Vetel & Le Gall, 2006). Closing the velocity budget to the east of XTBI suggests that 2–3 mm/year of extension could be occurring across the Ririba Rift and the southern portion of the Chew Bahir. The Kino Sogo fault zone has also been cited as a region of ongoing extension, between stations XTBI and MARS (Key & Watkins, 1988; Vetel et al., 2005; Vetel & Le Gall, 2006). Assuming similar extension rates along the length of the lake, 1–2 mm/year of extension could be occurring across the Kino Sogo and Chalbi desert regions, though the role of individual structures in this area is unresolved due to limited station distribution. The Chalbi desert is a former lake basin between the <2.5 Ma, large shield complexes of Kulal, Marsabit, and Hurri Hills during the Pleistocene (Bruhn et al., 2011), attesting to a phase of vertical crustal movements during the past 2.5 Myr of volcanism on the eastern side of Lake Turkana.

South of the Turkana Depression, extension is partitioned between the parallel Western and Eastern rifts. The Suguta Rift sector, cited as an additional active segment in northern Kenya (Bosworth & Maurin, 1993; Vetel & Le Gall, 2006), lies south of the southern tip of Lake Turkana. The stations STRI and SEOL straddle the Suguta rift and measure 2–3 mm/year of extension between them. The relaying of extension between the Western and Eastern rifts has been documented in previous studies and suggest rates decreasing southward in the Eastern Rift, while rates increase southward in the Western Rift (Stamps et al., 2008; Saria et al., 2014).

The overall kinematics of the region includes an extensional budget shared between the Ethiopian Highlands and the MER in the northern part of the study area and continuing as far south as the Ethiopia-Kenya border. In the Turkana Depression, extension is localized across comparatively narrow zones of faults and eruptive volcanic centers. Lake Turkana-bounding faults serve as a kinematic bridge between the southernmost MER and the northernmost portion of the Eastern rift. Effectively at least half of the total Nubia-Somalia relative motion from the Afar triple junction to around latitude 3°N is accommodated across a relatively narrow continuous rift domain. South of Lake Turkana, a portion of the total Nubia-Somalia velocity is partitioned to the Western rift along as yet unidentified structures, and perhaps as a broad zone of distributed strain.

4.2. Dynamics

The study region also provides an opportunity to test the relative importance of GPE and lateral mechanical heterogeneity in controlling the style of extension (Figure 1). Distributed deformation in the Ethiopian Highlands has been linked to gradients in GPE related to the topography (Birhanu et al., 2016) and to lateral mechanical heterogeneity (rheology) (Jay et al., 2015). Following this hypothesis, the lack of topographic gradients in the Turkana Depression predicts the observed shift to localized rifting (Figure 1—dashed lines represent the plateau extents). In the north of the Depression, extension occurs on both a highly localized rift structure and elsewhere west of the along-strike extension of the MER, either across the Omo Basin or throughout the southernmost high topography of the Ethiopian Plateau. In southern Turkana, where high elevation terrain is entirely absent, extension is entirely localized to Lake Turkana. These results indicate that GPE, or the lack of GPE in the case of the Turkana Depression, influences the scaling of active rifting. However, using surface observations alone, it is impossible to deconvolve force balance and rheology (Bendick & Flesch, 2013).

The relay from hybrid extension in the MER to higher strain rate and localized extension in the Turkana Depression also precludes distributed stretching related to preexisting crustal weaknesses or obliquity of the Depression, as proposed in some models of the study area (Agostini et al., 2009; Brune, 2016; Corti, 2012). In particular, the Anza Graben has been cited as an inherited structure that could influence strain partitioning in the Turkana Depression (Figure 1) (Brune, 2016), but the Anza Graben appears to be aseismic, and lacks morphological evidence for young faults (e.g., Vetel & Le Gall, 2006). The length scale over which strain is accommodated in the Turkana Depression is only tens of kilometers (Figure 4) and finite strain rates do not extend into or toward the Anza Graben.

In Kenya profile, the length scale of rifting is narrower than in the MER and comparable to that in the Turkana Depression (Figure 4), but only if the contribution of the Western Rift is ignored. The Kenya profile in this study is not capturing the complete divergence of Nubia-Somalia, but is instead measuring only extension across the Eastern rift. Therefore, while the Eastern Rift alone has a characteristic length scale similar to the Turkana Depression, the EARS south of the Depression accommodates divergence across two rift systems whose combined characteristic scale is equal to or greater than that in Ethiopia. Additionally, large uncertainties in velocities from within the East African Plateau make it difficult to determine if small amounts of extension are being accommodated within the Kenyan Plateau as in the Ethiopian Highlands, or if extension is confined to the Eastern and Western Rifts.

5. Conclusion

Comparing the deformation of the Turkana Depression to rift segments to its north and south, we find a systematic pattern of extensional accommodation. Forty to one hundred percent of the total Nubia-Somalia relative velocity is accommodated on high-strain rate, localized structures. The remainder of the total relative velocity is accommodated at lower strain rates over at least part of the elevated African plateaux. Where there is no high topography, such as in the Turkana Depression, extension focuses onto a narrow region with one or few crustal-scale dislocations and volcanic centers. The high-strain-rate fault-like part of the Turkana Depression bridges the MER and Eastern Rift as an effectively through-going single structure.

Where present, the component of distributed stretching superimposed and augmenting the localized rifting appears to be related to the convolution of GPE with lithospheric material properties. Where topographic gradients are large and the crust is thick, low strain rate stretching extends well outside the structural rift

and accommodates as much extension as the rift itself. Where high topography is absent and the crust is thin, stretching is restricted onto a localized single structure. The exact proportion of stretching accommodated by each mechanism is likely to be related both to the characteristic scaling of the gravitational body force and the material properties of the lithosphere, but these cannot be uniquely differentiated by surface observations alone. The tectonic history of the Turkana Depression suggests, however, that inherited crustal mechanical heterogeneity does not itself produce distributed deformation because the present-day strain field in the Depression shows little or no influence from well-documented inherited fault and basin systems. However, inherited weaknesses could certainly influence the specific location of the present-day high-strain-rate structures.

Acknowledgments

This research was supported by NSF grants 1824199, 1824417, 17277277, and 1551823. UNAVCO provided technical support and data services. Ethiopian fieldwork and logistics was greatly improved thanks to EthioDer Tours and Travel, especially by Eyaya Demessie. We thank the Turkana Basin Institute for logistical help and hosting two continuous GPS stations in Kenya. We appreciate Bob Reynolds willingness to download data in remote locations and showing author EK the geology of Turkana. All data are available from the UNAVCO archive in compliance with the AGU data policy (<https://www.unavco.org/data/gps-gnss/gps-gnss.html>). This study utilized data from stations supported by the African Geodetic Reference Frame (AFREF) and the Regional Center for Mapping and Development in Kenya including stations RCMN and DKUT. Additional reference stations data are provided by International GNSS Service (IGS). The solution was also combined with MIT's community velocity solution, which includes publicly available data made possible by many different research groups under the solution doi:10.1594/IEDA/324785.

References

- Agostini, A., Corti, G., Zeoli, A., & Mulugeta, G. (2009). Evolution, pattern, and partitioning of deformation during oblique continental rifting: Inferences from lithospheric-scale centrifuge models. *Geochemistry, Geophysics, Geosystems*, *10*, Q11015. <https://doi.org/10.1029/2009GC002676>
- Altamimi, Z., Métivier, L., & Collilieux, X. (2012). ITRF2008 plate motion model. *Journal of Geophysical Research*, *117*, B07402. <https://doi.org/10.1029/2011JB008930>
- Altamimi, Z., Rebeschung, P., Métivier, L., & Collilieux, X. (2016). ITRF2014: A new release of the International Terrestrial Reference Frame modeling nonlinear station motions. *Journal of Geophysical Research: Solid Earth*, *121*, 6109–6131. <https://doi.org/10.1002/2016JB013098>
- Altamimi, Z., Métivier, L., Rebeschung, P., Rouby, H., & Collilieux, X. (2017). ITRF14 plate motion model. *Geophysical Journal International*, *209*, 1906–1912. <https://doi.org/10.1093/gji/ggx136>
- Balestrieri, M. L., Bonini, M., Corti, G., Sani, F., & Philippon, M. (2016). A refinement of the chronology of rift-related faulting in the Broadly Rifted Zone, southern Ethiopia, through apatite fission-track analysis. *Tectonophysics*, *671*, 42–55. <https://doi.org/10.1016/j.tecto.2016.01.012>
- Bastow, I. D., Nyblade, A. A., Stuart, G. W., Rooney, T. O., & Benoit, M. H. (2008). Upper mantle seismic structure beneath the Ethiopian hot spot: Rifting at the edge of the African low-velocity anomaly. *Geochemistry, Geophysics, Geosystems*, *9*, Q12022. <https://doi.org/10.1029/2008GC002107>
- Bendick, R., & Flesch, L. (2013). A review of heterogeneous material and their implication for relationships between kinematics and dynamics in continents. *Tectonics*, *32*, 980–992. <https://doi.org/10.1002/tect.20058>
- Birhanu, Y., Bendick, R., Fisseha, S., Lewi, E., Floyd, M., King, R., & Reilinger, R. (2016). GPS constraints on broad scale extension in the Ethiopian Highlands and Main Ethiopian Rift. *Geophysical Research Letters*, *43*, 6844–6851. <https://doi.org/10.1002/2016GL069890>
- Bonini, M., Corti, G., Innocenti, F., Manetti, P., Mazzarini, F., & Abebe, T. (2005). Evolution of the Main Ethiopian Rift in the frame of Afar and Kenya rifts propagation. *Tectonics*, *24*, TC1007. <https://doi.org/10.1029/2004TC001680>
- Boone, S. C., Kohn, B. P., Gleadow, A. J., Morley, C. K., Seiler, C., & Foster, D. A. (2019). Birth of the East African Rift System: Nucleation of magmatism and strain in the Turkana Depression. *Geology*, *47*(9), 886–890.
- Boone, S. C., Seiler, C., Kohn, B. P., Gleadow, A. J. W., Foster, D. A., & Chung, L. (2018). Influence of rift superposition on lithospheric response to East African Rift System extension: Lapur Range, Turkana, Kenya. *Tectonics*, *37*, 182–207. <https://doi.org/10.1002/2017TC004575>
- Bosworth, W. (1992). Mesozoic and early Tertiary rift tectonics in East Africa. *Tectonophysics*, *209*(1-4), 115–137. [https://doi.org/10.1016/0040-1951\(92\)90014-W](https://doi.org/10.1016/0040-1951(92)90014-W)
- Bosworth, W., & Maurin, A. (1993). Structure, geochronology and tectonic significance of the northern Suguta Valley (Gregory Rift), Kenya. *Journal of the Geological Society of London*, *150*, 751–763. <https://doi.org/10.1144/gsjgs.150.4.0751>
- Bosworth, W., & Morley, C. K. (1994). Structural and stratigraphic evolution of the Anza rift, Kenya. *Tectonophysics*, *236*(1-4), 93–115. [https://doi.org/10.1016/0040-1951\(94\)90171-6](https://doi.org/10.1016/0040-1951(94)90171-6)
- Brown, F. H., & McDougall, I. (2011). Geochronology of the Turkana Depression of Northern Kenya and Southern Ethiopia. *Evolutionary Anthropology*, *20*, 217–227.
- Bruhn, R. L., Brown, F. H., Gathogo, P. N., & Haileab, B. (2011). Pliocene volcano-tectonics and paleogeography of the Turkana Basin, Kenya and Ethiopia. *Journal of African Earth Sciences*, *59*, 295–312. <https://doi.org/10.1016/j.jafrearsci.2010.12.002>
- Brune, S., Corti, G., & Ranalli, G. (2017). Controls of inherited lithospheric heterogeneity on rift linkage: Numerical and analog models of interaction between the Kenyan and Ethiopian rifts across the Turkana depression. *Tectonics*, *36*, 1767–1786. <https://doi.org/10.1002/2017TC004739>
- Brune, S. (2016). Rifts and rifted margins: A review of geodynamic processes and natural hazards. In J. C. Duarte, & W. P. Schellart (Eds.), *Plate boundaries and natural hazards, Geophysical Monograph Series*, (Vol. 219, pp. 11–37). Hoboken, NJ: John Wiley
- Chambers, E. L., Harmon, N., Keir, D., & Rychert, C. A. (2019). Using ambient noise to image the northern East African Rift. *Geochemistry, Geophysics, Geosystems*, *20*, 2091–2109. <https://doi.org/10.1029/2018GC008129>
- Coblentz, D. D., & Sandiford, M. (1994). Tectonic stresses in the African plate: Constraints on the ambient lithospheric stress state. *Geology*, *22*, 831–834.
- Corti, G. (2009). Continental rift evolution: From rift initiation to incipient break-up in the Main Ethiopian rift, East Africa. *Earth-Science Reviews*, *96*, 1–53.
- Corti, G. (2012). Evolution and characteristics of continental rifting: Analogue modeling-inspired view and comparison with examples from the East African Rift System. *Tectonophysics*, *522*–523, 1–33. <https://doi.org/10.1016/j.tecto.2011.06.010>
- Corti, G., Molin, P., Sembroni, A., Bastow, I. D., & Keir, D. (2018). Control of pre-rift lithospheric structure on the architecture and evolution of continental rifts: Insights from the Main Ethiopian Rift, East Africa. *Tectonics*, *37*, 477–496. <https://doi.org/10.1002/2017TC004799>
- Davidson, A., & Rex, D. C. (1980). Age of volcanism and rifting in southern Ethiopia. *Nature*, *283*, 657–658. <https://doi.org/10.1038/283657a0>

- DeMets, C., Gordon, R. G., & Argus, D. F. (2010). Geologically current plate motions. *Geophysical Journal International*, *181*, 1–80. <https://doi.org/10.1111/j.1365-246X.2009.04491.x>
- DeMets, C., & Merkouriev, S. (2016). High-resolution estimates of Nubia–Somalia plate motion since 20 Ma from reconstructions of the Southwest Indian Ridge, Red Sea and Gulf of Aden. *Geophysical Journal International*, *207*(1), 317–332.
- Dunkelman, T., Rosendahl, B. R., & Karson, J. A. (1989). Structure and stratigraphy of the Turkana rift from seismic reflection data. *Journal of African Earth Sciences*, *8*, 489–510. [https://doi.org/10.1016/S0899-5362\(89\)80041-7](https://doi.org/10.1016/S0899-5362(89)80041-7)
- Ebinger, C. (1989). Tectonic development of the western branch of the East African rift system. *Geological Society of America Bulletin*, *10*, 885–903. [https://doi.org/10.1130/00167606\(1989\)101<0885:TDOTWB>2.3.CO;2](https://doi.org/10.1130/00167606(1989)101<0885:TDOTWB>2.3.CO;2)
- Ebinger, C., & Sleep, N. (1998). Cenozoic magmatism throughout East Africa resulting from impact of a single plume. *Nature*, *395*, 788–791. <https://doi.org/10.1038/283657a0>
- Ebinger, C., Yemane, T., Harding, D., Tesfaye, S., Kelley, S., & Rex, D. (2000). Rift deflection, migration, and propagation: Linkage of the Ethiopian and Eastern Rifts, Africa. *Memoir - Geological Society of America*, *112*, 163–176. [https://doi.org/10.1130/0016-7606\(2000\)112<163:RDMAPL>2.0.CO;2](https://doi.org/10.1130/0016-7606(2000)112<163:RDMAPL>2.0.CO;2)
- Ebinger, C., Yemane, T., Woldegabriel, G., Aronson, J., & Walter, R. (1993). Late Eocene-recent volcanism and faulting in the southern main Ethiopian rift. *Journal of the Geological Society*, *150*, 99–108. <https://doi.org/10.1144/gsjgs.150.1.0099>
- Ebinger, C. J., & Ibrahim, A. (1994). Multiple episodes of rifting in central and east Africa: A re-evaluation of gravity data. *Geologische Rundschau*, *83*(4), 689–702. <https://doi.org/10.1007/BF00251068>
- Ebinger, C. J., Keir, D., Bastow, I. D., Whaler, K., Hammond, J. O. S., Ayele, A., & Hautot, S. (2017). Crustal structure of active deformation zones in Africa: Implications for global crustal processes. *Tectonics*, *36*, 3298–3332. <https://doi.org/10.1002/2017TC004526>
- Furman, T., Bryce, J. G., Karson, J., & Iotti, A. (2004). East African Rift System (EARS) plume structure: Insights from Quaternary mafic lavas of Turkana, Kenya. *Journal of Petrology*, *45*(5), 1069–1088. <https://doi.org/10.1093/petrology/egh004>
- Furman, T., Bryce, J. G., Rooney, T., Hanan, B. B., Yirgu, G., & Ayalew, D. (2006). Heads and tails: 30 million years of the Afar plume. In G. Yirgu, C. Ebinger, & P. Maguire (Eds.), *The Afar Volcanic Province Within the East African Rift System* (Vol. 259, pp. 95–120). London: Geological Society Special Publication. <https://doi.org/10.1144/GSL.SP.2006.259.01.09>
- George, R., Rogers, N., & Kelley, S. (1998). Earliest magmatism in Ethiopia: Evidence for two mantle plumes in one flood basalt province. *Geology*, *26*, 923–926. [https://doi.org/10.1130/0091-7613\(1998\)026<0923:EMIEEF>2.3.CO;2](https://doi.org/10.1130/0091-7613(1998)026<0923:EMIEEF>2.3.CO;2)
- Guth, A. L. (2016). Volcanic volumes associated with the Kenya Rift: Recognition and correction of preservation biases. *Geological Society of London, Special Publication*, *420*, 31–42. <https://doi.org/10.1144/SP420.3>
- Hendrie, D. B., Kusznir, N. J., Morley, C. K., & Ebinger, C. J. (1994). Cenozoic extension in northern Kenya: A quantitative model of rift basin development in the Turkana region. *Tectonophysics*, *236*(1), 409–438. [https://doi.org/10.1016/0040-1951\(94\)90187-2](https://doi.org/10.1016/0040-1951(94)90187-2)
- Herring, T., King R., & McClusky S. (2010). Introduction to GAMIT/GLOBK Release 10.4. Mass. Inst. of Technol., Cambridge.
- Jay, C., Flesch L. M., & Bendick R. (2015). Kinematics and dynamics of the Main Ethiopian Rift, AGU Fall Meeting Abstracts.
- Kaesser, B., Kalt, A., & Pettke, T. (2006). Evolution of the lithospheric mantle beneath the Marsabit volcanic field (Northern Kenya): Constraints from textural, P-T and geochemical studies on xenoliths. *Journal of Petrology*, *47*. <https://doi.org/10.1093/petrology/eg1040>
- Kendall, J.M., and C. Lithgow-Bertelloni (2016). Why is Africa rifting? From: Wright, T. J., Ayele, A., Ferguson, D. J., Kidane, T. & Vye-Brown, C. (Eds.). *Magmatic Rifting and Active Volcanism* (420, 11–30). London, England: Geological Society Special Publication.
- Key, R. M., & Watkins, R. T. (1988). Geology of the Sabarei area. *Kenya Mines and Geol. Dep. Rep.*, *111*, 57 pp. A.F.
- King, R., Floyd, M., Reilinger, R., & Bendick, R. (2019). GPS velocity field (MIT 2019.0) for the East African Rift System generated by King et al. Interdisciplinary Earth Data Alliance (IEDA). DOI: <https://doi.org/10.1594/IEDA/324785>.
- Kogan, L., Fisseha, S., Bendick, R., Reilinger, R., McClusky, S., King, R., & Solomon, T. (2012). Lithospheric strength and strain localization in continental extension from observations of the East African Rift. *Journal of Geophysical Research*, *117*, B03402. <https://doi.org/10.1029/2011JB008516>.Mackenzie
- Mechie, J., Keller, G. R., Prodehl, C., Gaciri, S., Braile, L. W., Mooney, W. D., et al. (1994). Crustal structure beneath the Kenya Rift from axial profile data. *Tectonophysics*, *236*(1-4), 179–200. [https://doi.org/10.1016/0040-1951\(94\)90176-7](https://doi.org/10.1016/0040-1951(94)90176-7)
- Morley, C. K., Day, R. A., Lauck, R., Bosher, R., Stone, D. M., Wigger, S. T., et al. (1999). Geology and Geophysics of the Anza Graben. In C. K. Morley (Ed.), *Geoscience of Rift Systems-Evolution of East Africa*, AAPG Studies in Geology (Vol. 44, pp. 67–90). Tulsa, OK: The American Association of Petroleum Geologists.
- Morley, C. K., Wescott, W. A., Stone, D. M., Harper, R. M., Wigger, S. T., & Karanja, F. M. (1992). Tectonic evolution of the northern Kenya rift. *Journal of the Geological Society*, *149*, 333–348. <https://doi.org/10.1144/gsjgs.149.3.0333>
- Morley, C. K., Wescott, W. A., Stone, D. M., Harper, R. M., Wigger, S. T., Karanja, F. M., & Day, R. A. (1999). Geology and geophysics of the western Turkana basins. In C. K. Morley (Ed.), *Geoscience of Rift Systems-Evolution of East Africa*, AAPG Studies in Geology (Vol. 44, pp. 19–54). Tulsa, OK: The American Association of Petroleum Geologists.
- Pik, R., Marty, B., Carignan, J., Yirgu, G., & Ayalew, T. (2008). Timing of East African Rift development in southern Ethiopia: Implication for mantle plume activity and evolution of topography. *Geology*, *36*(2), 167–170. <https://doi.org/10.1130/G24233A.1>
- Reilinger, R., McClusky, S., Vernant, P., Lawrence, S., Ergintav, S., & Cakmak, R. (2006). GPS constraints on continental deformation in the Africa-Arabia-Eurasia continental collision zone and implications for the dynamics of Plate interactions. *Journal of Geophysical Research*, *111*, B05411. <https://doi.org/10.1029/2005JB004051>
- Rooney, T. O. (2017). The Cenozoic magmatism of East-Africa: Part 1—Flood basalts and pulsed magmatism. *Lithos*, *286-287*, 264–301. <https://doi.org/10.1016/j.lithos.2017.05.014>
- Saria, E., Calais, E., Altamimi, Z., Willis, P., & Farah, H. (2013). A new velocity field for Africa from combined GPS and DORIS space geodetic solutions: Contribution to the definition of the African reference frame (AFREF). *Journal of Geophysical Research - Solid Earth*, *118*, 1677–1697. <https://doi.org/10.1002/jgrb.50137>
- Saria, E., Calais, E., Stamps, D. S., Delvaux, D., & Hartnady, C. J. H. (2014). Present-day kinematics of the East African Rift. *Journal of Geophysical Research: Solid Earth*, *119*(4), 3584–3600. <https://doi.org/10.1002/2013jb010901>
- Sippel, J., Meeßen, C., Cacace, M., Mechie, J., Fishwick, S., Heine, C., & Strecker, M. R. (2017). The Kenya Rift revisited: Insights into lithospheric strength through data-driven 3-D gravity and thermal modeling. *Solid Earth*, *8*(1), 45–81. <https://doi.org/10.5194/se-8-45-2017>
- Stamps, D. S., Calais, E., Saria, E., Hartnady, C., Nocquet, J. M., Ebinger, C. J., & Fernandes, R. M. (2008). A kinematic model for the East African rift. *Geophysical Research Letters*, *35*(L05304). <https://doi.org/10.1029/2007GL03278>
- Stamps, S., Flesch, L., Calais, E., & Ghosh, A. (2014). Current kinematics and dynamics of Africa and the East African Rift System. *Journal of Geophysical Research - Solid Earth*, *119*, 5161–5186. <https://doi.org/10.1002/2013JB010717>

- Tiercelin, J.-J., Potdevin, J. L., Thuo, P. K., Abdelfettah, Y., Schuster, M., Bourquin, S., et al. (2012). Stratigraphy, sedimentology and diagenetic evolution of the Lapur Sandstone in northern Kenya: Implications for oil exploration of the Meso-Cenozoic Turkana depression. *Journal of African Earth Sciences*, 71-72, 43–79.
- Vetel, W., & Le Gall, B. (2006). Dynamics of prolonged continental extension in magmatic rifts: The Turkana Rift case study (North Kenya). *Geological Society of London, Special Publication*, 259(1), 209–233. <https://doi.org/10.1144/GSL.SP.2006.259.01.17>
- Vetel, W., Le Gall, B., & Walsh, J. J. (2005). Geometry and growth of an inner rift fault pattern: The Kino Sogo Fault Belt, Turkana Rift (North Kenya). *Journal of Structural Geology*, 27(12), 2204–2222. <https://doi.org/10.1016/j.jsg.2005.07.003>
- Wescott, W. A., Wigger, S. T., Stone, D. M., & Morley, C. K. (1999). Geology and Geophysics of the Lotikipi Plain. In C. K. Morley (Ed.), *Geoscience of Rift Systems-Evolution of East Africa, AAPG Studies in Geology* (Vol. 44, pp. 55–66). Tulsa OK: The American Association of Petroleum Geologists.
- Wolfenden, E., Ebinger, C., Yirgu, G., Deino, A., & Ayalew, D. (2004). Evolution of the northern Main Ethiopian Rift: Birth of a triple junction. *Earth and Planetary Science Letters*, 224, 213–222. <https://doi.org/10.1016/j.epsl.2004.04.022>

References From the Supporting Information

- Baker, B. H., & Wohlenberg, J. (1971). Structure and evolution of the Kenya Rift Valley. *Nature*, 229(5286), 538–542. <https://doi.org/10.1038/229538a0>
- Ebinger, C. J., & Casey, M. (2001). Continental breakup in magmatic provinces: An Ethiopian example. *Geology*, 29, 527–530. [https://doi.org/10.1130/00917613\(2001\)029](https://doi.org/10.1130/00917613(2001)029)
- Ibrahim, A. (1993). Interpretation of gravity and magnetic data from the Central African rift system, Sudan, PhD Thesis, Univ Leeds, 208.
- McDougall, I., & Brown, F. H. (2009). Timing of volcanism and evolution of the northern Kenya Rift. *Geological Magazine*, 146, 34–47. <https://doi.org/10.1017/S0016756808005347>
- McDougall, I., & Watkins, R. T. (2006). Geochronology of the Nabwal Hills: A record of earliest magmatism in northern Kenyan Rift Valley. *Geological Magazine*, 143, 25–39. <https://doi.org/10.1017/S0016756805001184>
- Rooney, T., Furman, T., Bastow, I., Ayalew, D., & Yirgu, G. (2007). Lithospheric modification during crustal extension in the Main Ethiopian Rift. *Journal of Geophysical Research*, 112, B10201. <https://doi.org/10.1029/2006JB004916.1>
- Watkins, R. T. (1986). Volcano-tectonics control on sedimentation in the Koobi Fora sedimentary basin, Lake Turkana. In L. E. Frostick, R. W. Renaut, I. Read, & J. J. Tiercelin (Eds.), *Sedimentation in the African Rifts, Geological Society London Special Publications*, no. 25, (pp. 85–94). Oxford: Blackwell Scientific Publications.